

Dynamics of the geometric phase in inhomogeneous quantum spin chains

Kaiyuan Cao[✉], Shuxiang Yang, and Yayun Hu^{*}

Research Center for Intelligent Supercomputing, Zhejiang Lab, Hangzhou 311100, People's Republic of China

Guangwen Yang[†]

Research Center for Intelligent Supercomputing, Zhejiang Lab, Hangzhou 311100, People's Republic of China

and Department of Computer Science and Technology, Tsinghua University, Haidian District, Beijing 100084, People's Republic of China



(Received 3 January 2023; revised 30 May 2023; accepted 26 June 2023; published 5 July 2023; corrected 12 July 2023)

The dynamics of the geometric phase are studied in inhomogeneous quantum spin chains after a quench. Analytic expressions of the Pancharatnam geometric phase (PGP) are derived for both the period-2 quantum Ising chain (QIC) and the disordered QIC. In the period-2 QIC, due to the periodic modulation, the phase difference between the boundaries of the half Brillouin zone $(0, \pi]$ changes with time, and consequently, the winding number $\nu_D(t)$ of the PGP is not quantized and thus is not topological anymore. Nevertheless, the PGP and its winding number show nonanalytic singularities at the critical times of the dynamical quantum phase transitions (DQPTs). This relation between the PGP and the DQPT is further confirmed in the disordered QIC. It is found that the critical time of the DQPT inherited from the homogeneous system and the additional one induced by weak disorder are also accompanied by the nonanalytic singularity of the PGP by decomposing the PGP into each quasiparticle mode. The connection between the nonanalytic behavior of the PGP at the critical time and the DQPT, regardless of whether the winding number is topological, can be explained by the fact that they both arise when the Loschmidt amplitude vanishes.

DOI: [10.1103/PhysRevB.108.024201](https://doi.org/10.1103/PhysRevB.108.024201)

I. INTRODUCTION

The geometric phase has seen remarkable advancements [1–3] since Berry published his seminal paper [4], in which a quantum system is subjected to an adiabatically changing environment and manifests a geometric behavior in its phase [5]. The Berry phase encodes the state of the system and has been associated with a variety of condensed matter phenomena, such as the quantum Hall effect [6] and quantum phase transitions [7,8]. Later, the concept of Berry's phase was generalized to the cyclic evolution of the quantum system [9] and to an even more general context that is neither unitary nor cyclic, which is known as the Pancharatnam geometric phase (PGP) [10]. Recently, the PGP was proposed to characterize the dynamical quantum phase transition (DQPT) [11].

The DQPT describes the nonanalytic behavior of the Loschmidt echo $\mathcal{L}(t) = |\mathcal{G}(t)|^2$ during the nonequilibrium dynamical evolution [12,13], where the Loschmidt amplitude $\mathcal{G}(t)$ measures the overlap of the time-evolving state with the initial state, i.e.,

$$\mathcal{G}(t) = \langle \psi_0 | \psi(t) \rangle = \langle \psi_0 | e^{-iHt} | \psi_0 \rangle. \quad (1)$$

Like for the equilibrium phase transition, one can define the dynamical free energy density by the rate function $\lambda(t) = -\lim_{N \rightarrow +\infty} \frac{1}{N} \ln [\mathcal{L}(t)]$, which shows the cusplike singularities at the critical times of DQPTs [14]. To date, the DQPT has

been studied extensively in many quantum systems, such as XY chains [15–17], the Kitaev honeycomb model [18], XXZ model [19,20], systems with long-range interactions [21–26], quantum Potts model [27], non-Hermitian systems [28,29], the Bose-Einstein condensate [30], and inhomogeneous systems [31–34]. Moreover, direct observations of DQPTs have been realized in many experiments, such as trapped ions simulations [35], a 53-qubit quantum simulation [36], a nuclear magnetic resonance quantum simulator [37], quantum walks of photons [38,39], and spinor condensate simulations [40]. Note that another different definition of the DQPT exists that studies the asymptotic late-time steady state of the order parameter [41–45]. Two types of DQPTs have been found related to the long-range quantum Ising chain [26].

According to Berry's theory, a quantum system acquires a geometric phase $\phi^G(t)$ over the dynamical phase $\phi^{\text{dyn}}(t)$ during the time evolution [4]. The PGP [10,11] can be calculated as

$$\phi^G(t) = \phi(t) - \phi^{\text{dyn}}(t), \quad (2)$$

with the total phase $\phi(t) = \arg[\mathcal{G}(t)]$ and $\phi^{\text{dyn}}(t) = -\int_0^t ds \langle \psi(s) | H | \psi(s) \rangle$. One can define the winding number $\nu_D(t) = \int_0^\pi [\partial \phi_k^G(t) / \partial k] dk / 2\pi$, which is found to be integer quantized between two critical times and changes by unity at critical times, so that the winding number is treated as the dynamical topological order parameter (DTOP) [11]. The PGP shows nonanalytic singularities as dynamical vortices at the critical times of DQPTs [46,47]. The DTOP has been confirmed in many works, for instance, slow

^{*}hyy@zhejianglab.com

[†]ygw@tsinghua.edu.cn

quench in the quantum Ising chain [48], the \mathcal{PT} -symmetric Su-Schrieffer-Heeger model [49], the massive Schwinger model [50], systems under periodic driving [51–57], and others [25,28,38,39]. However, clear evidence shows that the winding number $\nu_D(t)$ may be fractional quantized and thus nontopological in the XY chain from a critical quantum quench [58], although the discontinuous point of $\nu_D(t)$ is still one to one related to the DQPT. A significant question that follows is whether the DQPT and its associated PGP are always accompanied by an integer-quantized (topological) winding number in general.

To answer this question, we investigate the PGP in two inhomogeneous systems: the period-2 quantum Ising chain (QIC) and the disordered QIC. It is well known that inhomogeneity can dramatically influence the behavior of DQPT [33,59]. The periodic modulation is found to induce richer DQPTs than those in the homogeneous system [59]. New DQPTs appear after a quench across the critical lines of the quantum phase transition under the influence of weak disorder [33]. Another ensuing interesting problem is whether the new extra DQPTs induced by the periodic modulation and the disorder are also related to the singularity of the PGP and its winding number. This is, indeed, the case in our work. The results reveal that the critical times of DQPTs induced by the periodic modulation and weak disorder can still be characterized by the nonanalytic singularity of the PGP. This can be understood from the fact that the vanishing of the Loschmidt amplitude contributes not only a cusp in the rate function for the DQPT but also a dynamical vortex for the PGP.

However, in the period-2 QIC, the winding number $\nu_D(t)$ is found not to be quantized anymore, although it still shows discontinuities at the critical times of DQPTs. The reason for the nonquantized winding numbers can be explained as the phase difference $\phi_{k=\pi}^G(t) - \phi_{k=0}^G(t)$ between the PGPs at the boundaries changing with time due to periodic modulation. This is different from the case in the XY chain from a critical quench [58], in which the fractional-quantized winding numbers are related to the singularity of the Bogoliubov angle at the gap-closing momentum.

This paper is organized in the following manner: in Sec. II, we discuss the QIC with period-2 nearest-neighbor interactions and give the formulas for the PGP and its winding number (more detailed derivations are given in Appendix), and we study the behavior of the PGP via two typical quench processes. In Sec. III, we derive the PGP of the disordered QIC in real space (more detailed derivations are given in Appendix B); similarly, we give two typical examples to illustrate the behavior of the PGP in the disordered system. Finally, we summarize our results and draw our conclusions in Sec. IV.

II. PERIODIC QUANTUM SPIN CHAINS

We consider the quantum Ising chain with periodic nearest-neighbor interactions in the transverse field [59–62]. The Hamiltonian is given by

$$H = -\frac{1}{2} \sum_{n=1}^N J_n \sigma_n^x \sigma_{n+1}^x - \frac{\hbar}{2} \sum_{n=1}^N \sigma_n^z, \quad (3)$$

where σ^a ($a = x, y, z$) are the Pauli matrices, J_n is the strength of interactions between the nearest-neighbor spins, and \hbar is the external transverse field. We consider the QIC with period-2 nearest-neighbor interactions ($l \in \mathbb{Z}$),

$$J_n = \begin{cases} J, & n = 2l - 1, \\ J_1, & n = 2l. \end{cases} \quad (4)$$

For convenience, we set $\alpha = J_1/J$ and $J = 1$ without losing generality. The period-2 QIC undergoes the quantum phase transition from the ferromagnetic (FM) phase to the paramagnetic (PM) phase at the critical point $h_c = \sqrt{\alpha}$ when the external field h increases [60,63].

We can solve the Hamiltonian (3) via the Jordan-Wigner and Bogoliubov transformations (see Appendix A 1), where the diagonal form of the Hamiltonian is

$$H = \sum_k \Lambda_{k1} \left(\eta_{k1}^\dagger \eta_{k1} - \frac{1}{2} \right) + \Lambda_{k2} \left(\eta_{k2}^\dagger \eta_{k2} - \frac{1}{2} \right). \quad (5)$$

Unlike that in the homogeneous QIC, the period-2 QIC has two quasiparticle excitation spectra, Λ_{k1} and Λ_{k2} . The zero-point (ground-state) energy is given by

$$E_0 = \sum_{k>0} E_{0k} = - \sum_{k>0} (\Lambda_{k1} + \Lambda_{k2}), \quad (6)$$

and the ground state is $|\text{GS}\rangle = \bigotimes_{k>0} |\text{GS}_k\rangle$, with $|\text{GS}_k\rangle = |0_{k1}0_{-k1}0_{k2}0_{-k2}\rangle$ for every k ($k > 0$).

We study the nonequilibrium dynamical evolution induced by a quantum quench. The system is prepared in the ground state $|\psi_0\rangle = \bigotimes_{k>0} |\psi_{0k}\rangle$, $|\psi_{0k}\rangle = |\text{GS}_k\rangle$ of an initial Hamiltonian $H_0 = H(h_0)$. At time $t = 0$, the external field will be changed suddenly to another value, h_1 , that corresponds to the Hamiltonian $\tilde{H} = H(h_1)$. In this section, we use $\tilde{\eta}_k$ ($\tilde{\eta}_k^\dagger$), $|\tilde{\psi}_{0k}\rangle$, and $\tilde{\Lambda}_k$ to denote the corresponding items of the postquench Hamiltonian \tilde{H} . The time-evolved state is given by

$$|\psi_k(t)\rangle = e^{-i\tilde{H}t} |\psi_{0k}\rangle. \quad (7)$$

By decomposing the Loschmidt amplitude $\mathcal{G}(t) = \prod_{k>0} \mathcal{G}_k(t)$, we obtain

$$\mathcal{G}_k(t) = \frac{e^{-i\tilde{E}_{0k}t}}{\mathcal{N}^2} \prod_{\mu,\nu=1}^2 [1 + |G_{k\mu,-k\nu}|^2 e^{-i(\tilde{\Lambda}_{k\mu} + \tilde{\Lambda}_{-k\nu})t}], \quad (8)$$

where $G = -(U\tilde{U}^\dagger + V\tilde{V}^\dagger)^{-1}(U\tilde{V}^T + V\tilde{U}^T)$ is an antisymmetric matrix dependent on the parameters of the pre- and postquench Hamiltonian (see Appendix A 2). Like for the Lee-Yang zeros, we can illustrate the DQPT in a straightforward way via the Fisher zeros in the complex time plane [12]. From $\mathcal{G}_k(z) = 0$, $\text{Im}(z) = t$, the Fisher zeros of the Loschmidt amplitude for every k are given by

$$z_n(k, \mu, \nu) = \frac{1}{\tilde{\Lambda}_{k\mu} + \tilde{\Lambda}_{-k\nu}} [\ln |G_{k\mu,-k\nu}|^2 + i(2n + 1)\pi], \quad (9)$$

with $\mu, \nu = 1, 2$. The Fisher zeros will have an intersection with the imaginary axis of the complex time plane when the DQPT occurs. Equation (9) implies that Fisher zeros in the period-2 QIC have multiple branches which are different from the single branch in the homogeneous QIC [59]. With the help of the Fisher zeros (9), we can easily obtain the critical

momentum k_c of the DQPT which satisfies $|G_{k_c\mu, -k_c\nu}| = 1$ and the associated critical time

$$t_c(n) = \frac{(2n+1)\pi}{\tilde{\Lambda}_{k_c\mu} + \tilde{\Lambda}_{-k_c\nu}}. \quad (10)$$

To study the behavior of the PGP, we rewrite the Loschmidt amplitude $\mathcal{G}_k(t)$ in polar coordinates, which is

$$\mathcal{G}_k(t) = r_k(t)e^{i\phi_k(t)} = r_k(t)e^{i[\phi_k^{\text{dyn}}(t) + \phi_k^G(t)]}, \quad (11)$$

where $\phi_k^{\text{dyn}}(t)$ and $\phi_k^G(t)$ are the dynamical phase and purely geometric phase, respectively. According to Eq. (11), we get the dynamical free energy (rate function) in the thermodynamic limit as

$$\lambda(t) = - \int_0^\pi \frac{dk}{2\pi} \ln r_k^2(t). \quad (12)$$

Clearly, the rate function $\lambda(t)$ depends on only the modulus $r_k(t)$ of the Loschmidt amplitude $\mathcal{G}_k(t)$. However, at the critical momentum k_c , $\lambda(t)$ has a nonanalytic point, i.e., $r_{k_c}(t) = 0$. According to the basic theory in complex math, when a complex number has zero modulation, its argument angle can take any value. This will be reflected by a dynamical vortex (nonanalytic singularity) in the PGP [46,47]. This is the essential reason why DQPTs can be characterized by the PGP.

The PGP $\phi_k^G(t)$ can be extracted from the time-dependent argument $\phi_k(t)$ of the Loschmidt amplitude by

$$\phi_k^G(t) = \phi_k(t) - \phi_k^{\text{dyn}}(t), \quad (13)$$

where the dynamical phase $\phi_k^{\text{dyn}}(t)$ is

$$\begin{aligned} \phi_k^{\text{dyn}}(t) &= - \int_0^t ds \langle \psi(s) | \tilde{H}_k | \psi(s) \rangle \\ &= \left\{ \left[1 - \frac{2(|G_{k1, -k1}|^2 + |G_{k1, -k2}|^2)}{(1 + |G_{k1, -k1}|^2)(1 + |G_{k1, -k2}|^2)} \right] \tilde{\Lambda}_{k1} \right. \\ &\quad \left. + \left[1 - \frac{2(|G_{-k1, k2}|^2 + |G_{k2, -k2}|^2)}{(1 + |G_{-k1, k2}|^2)(1 + |G_{k2, -k2}|^2)} \right] \tilde{\Lambda}_{k2} \right\} t. \end{aligned} \quad (14)$$

The dynamical phase $\phi_k^{\text{dyn}}(t)$, which is found to be proportional to time t , is always an analytic function. Therefore, the nonanalytic behavior of the argument $\phi_k(t)$ will be reflected in the PGP $\phi_k^G(t)$ at the critical time, where $\phi_k^G(t)$ is ill defined.

Note that the PGP $\phi_k^G(t)$ is usually folded into its principal angle value, i.e., $\phi_k^G(t) \in (-\pi, \pi]$. One can define the winding number to describe the accumulated change of the PGP by

$$\nu_D = \frac{1}{2\pi} \int_0^\pi \frac{\partial \phi_k^G(t)}{\partial k} dk = \frac{\phi_{k=\pi}^G(t) - \phi_{k=0}^G(t)}{2\pi} + \mathcal{N}, \quad (15)$$

where \mathcal{N} is the folding number of the PGP from $-\pi$ to π or from π to $-\pi$ when $\phi_k^G(t)$ exceeds its principal value interval. The folding number decreases by one when the PGP is folded from $-\pi$ to π , and increases by one when folded from π to $-\pi$.

In the literatures [25,28,38,39,46,47,49–57,64–70], $\phi_k^G(t)$ are found pinned to zero at the boundary of the half Brillouin zone (or the whole Brillouin zone for topological insulators [28,54]) in the homogeneous systems, i.e., $\phi_{k=\pi}^G(t) - \phi_{k=0}^G(t) = 0$. This ensures that the winding number $\nu_D(t)$ is

integer quantized. However, the situation is different in our periodic case. It is found that the PGP changes value with time at the boundary of the half Brillouin zone under the periodic modulation, which results in the winding number not being quantized. In the following, we will show our interesting findings using two typical examples.

A. Quench from the FM phase to the PM phase

We further investigate the PGP $\phi_k^G(t)$ and the associated winding number $\nu_D(t)$ for the period-2 QIC by showing two typical quench examples. We take the value $\alpha = J_1/J = 0.5$, which implies the system undergoes an Ising transition at the critical point $h_c = \sqrt{\alpha} \approx 0.707$.

First, we study the case of quench from the FM phase to the PM phase. In Fig. 1(a), we show the contour plot of PGP $\phi_k^G(t)$ as a function of (k, t) , where the quench path is from $h_0 = 0.5$ to $h_1 = 2.0$. The symmetry of the Hamiltonian and the initial state ensures $\phi_k^G(t) = \phi_{-k}^G(t)$, so throughout this paper we show only the PGP in the (k, t) plane for $k > 0$. We obtain the critical momentum k_c and the critical times $t_c(n)$ of the DQPTs, which are marked by red crosses, according to Eqs. (9) and (10). Obviously, there is one critical momentum, $k_c \approx 1.10$, corresponding to multiple critical times, $t_c(n) = (2n+1)t_c(0)$, $n = 0, 1, \dots$ [see Fig. 1(a)]. It can be seen that ϕ_k^G has nonanalytic singularities (dynamical vortices circled in blue) at the critical times $t_c(n)$ and critical momentum k_c . Furthermore, we notice that $\phi_k^G(t)$ does not complete full circles in the half Brillouin zone, i.e., $\phi_{k=\pi}^G(t) - \phi_{k=0}^G(t) \neq 2n\pi$. For instance, when $t = 2$, $\phi_k^G(t)$ changes value by $0 \rightarrow -\pi \xrightarrow{\text{folding}} \pi \rightarrow 0.46\pi$ [see the blue line $t = 2$ in Fig. 1(a)]; when $t = 3.78$, $\phi_k^G(t)$ changes value by $0 \rightarrow -\pi \xrightarrow{\text{folding}} \pi \rightarrow -\pi \xrightarrow{\text{folding}} \pi$ [see the blue line $t = 3.78$ in Fig. 1(a)]. Here, $-\pi \xrightarrow{\text{folding}} \pi$ denotes restricting $\phi_k^G(t)$ to its principal angle value $(-\pi, \pi]$. This implies that the associated winding number $\nu_D(t)$ may not be an integer, according to Eq. (15).

To establish that this is, indeed, the case, we calculate and plot the winding number $\nu_D(t)$ as a function of t in Fig. 1(b). In order to see the critical times clearly, we also show the corresponding rate function $\lambda(t)$. It is clear that the winding number $\nu_D(t)$ is not integer quantized. Specifically, when $t = 2$, the winding number $\nu_D(t) \approx -0.77$ [see the blue line $t = 2$ in Fig. 1(b)]; when $t = 3.78$, $\nu_D(t) \approx -1.5$ [see the blue line $t = 3.78$ in Fig. 1(b)]. Nevertheless, the winding number $\nu_D(t)$ is to jump discontinuously at the critical times of the DQPTs. This means that the winding number can still detect the DQPTs even though it is not topological.

We now focus on three factor components of the PGP $\phi_k^G(t)$ for the momenta $k = 0$, $k = \pi$, and $k = k_c$ [see Figs. 2(a) and 2(b)], which are very relevant to $\nu_D(t)$ according to Eq. (15). It is found that at the boundary of the half Brillouin zone, $\phi_{k=0}^G(t) \approx 0$ remains almost constant all the time; however, $\phi_{k=\pi}^G(t)$ changes continuously with time. The phase difference $\phi_{k=\pi}^G(t) - \phi_{k=0}^G(t) \approx \phi_{k=\pi}^G(t)$ changes with time, and thus, the winding number cannot be integer quantized anymore. We tested other parameters and found this to be a general behavior in the case of quench from the FM phase to the PM phase (see Fig. 8 in Appendix A3). Note that the jump in $\phi_{k=\pi}^G(t)$ at time t^* results from restricting the

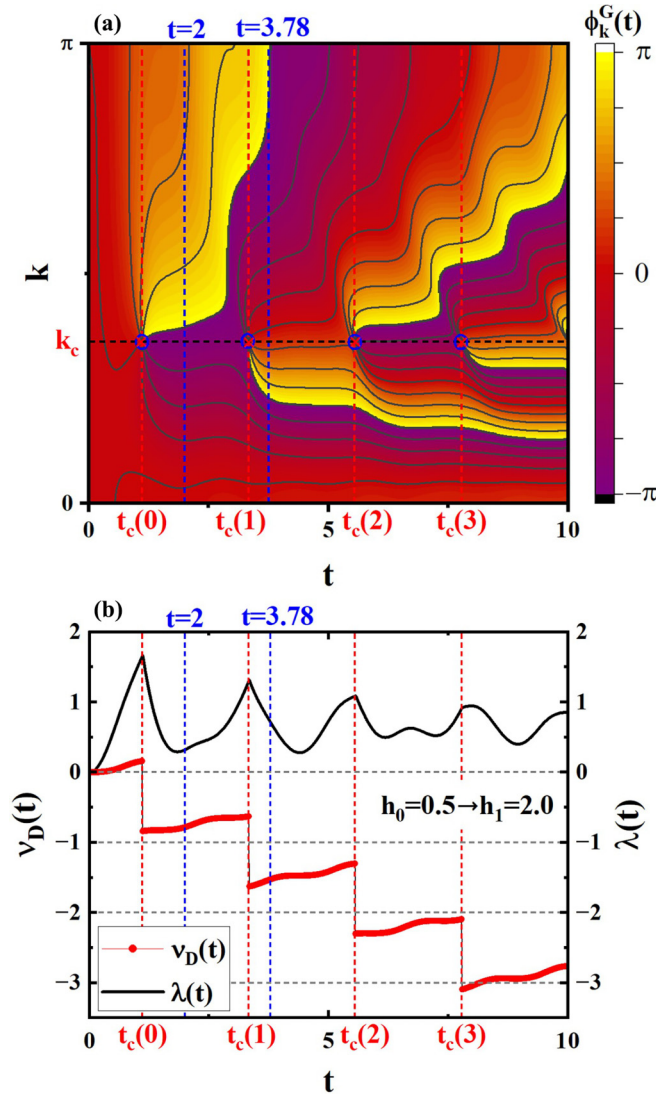


FIG. 1. (a) Contour plot of PGP $\phi_k^G(t)$ as a function of (k, t) for the quench from the FM phase to the PM phase ($h_0 = 0.5$ to $h_1 = 2.0$). The phase vortices are marked by blue circles at the critical momentum and critical times $(k_c, t_c(n))$. The red crosses denote the critical momenta and critical times obtained according to Eqs. (9) and (10). (b) The time evolutions of the winding number $v_D(t)$ (red squiggly lines) and the rate function $\lambda(t)$ (black line) are plotted for comparison. It can be seen that $v_D(t)$ is not integer quantized and jumps discontinuously at the critical times $t_c(n)$, $n = 0, 1, 2, 3, \dots$

PGP to its principal angle value, which will not lead to the presence of the DQPT. For the critical momentum $k_c \approx 1.10$ of the DQPT, we can see that $\phi_{k_c}^G(t)$ has nonanalytic points at times $t = t_c(0), t_c(1)$, which are exactly the critical times of the DQPT. In summary, the discontinuous integral jumps of the winding number result from the nonanalytic behaviors of the PGP at the critical times; the winding number is not quantized due to the time-dependent contribution from the PGP difference $\phi_{k=\pi}^G(t) - \phi_{k=0}^G(t)$.

B. Quench from the PM phase to the FM phase

As a second example, we consider the case of quench from the PM phase to the FM phase. In Fig. 3(a), we show

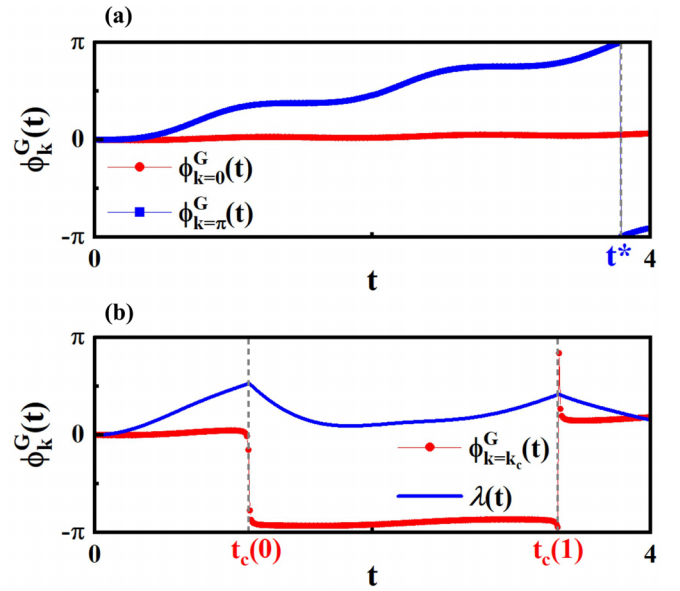


FIG. 2. Factor components of the PGP are plotted as a function of t (a) for $k = 0$ and $k = \pi$ and (b) for $k = k_c \approx 1.10$. At the boundary of the half Brillouin zone, $\phi_{k=0}^G(t) \approx 0$ is almost constant, but $\phi_{k=\pi}^G(t)$ changes value with time. Note that the jump of $\phi_{k=\pi}^G(t)$ at time t^* results from restricting the PGP to its principal angle value, which will not lead to the presence of the DQPT. However, for the critical momentum k_c , $\phi_{k_c}^G(t)$ shows nonanalytic singularities at critical times $t = t_c(0)$ and $t_c(1)$. The black line is the rate function $\lambda(t)$, which shows singularities at critical times $t = t_c(0)$ and $t_c(1)$.

the contour plot of the PGP $\phi_k^G(t)$ as a function of (k, t) . Here, the quench path is from $h_0 = 2.0$ to $h_1 = 0.5$, which is the inverse path of the previous example shown in the Figs. 1 and 2. Unlike that in the case of quench from the FM phase to the PM phase, there are three critical momenta, k_{c1}, k_{c2} , and k_{c3} , corresponding to three groups of critical times, $t_{c1}(n) = (2n + 1)t_{c1}(0)$, $t_{c2}(n) = (2n + 1)t_{c2}(0)$, and $t_{c3}(n) = (2n + 1)t_{c3}(0)$, $n = 0, 1, 2, \dots$. This can be understood based on Eq. (9); that is, three branches of Fisher zeros have intersections with the imaginary axis in the complex time plane [59]. At the critical momentum and critical times $(k_c, t_{cm}(n))$, $m = 1, 2, 3$, $\phi_k^G(t)$ has dynamical phase vortices, as circled in blue [see Fig. 3(a)]. Similar to the case of quench from the FM phase to the PM phase, $\phi_k^G(t)$ does not complete full circles in the half Brillouin zone. For instance, when $t = 0.53$, $\phi_k^G(t)$ changes value by $\pi \xrightarrow{\text{folding}} -\pi \rightarrow 0$, which implies the corresponding winding number $v_D(t = 0.53) \approx 0.5$. We plot the winding number $v_D(t)$ and rate function $\lambda(t)$ in Fig. 3(b). It can be seen that the winding number $v_D(t)$ shows an approximately linear change with time t within two neighboring critical times. As expected, the discontinuous points of $v_D(t)$ are accompanied by the critical times of DQPTs and the dynamical vortices in PGP [see Fig. 3(b)].

We also investigate the case of quench within the same phase in Appendix A3 (see Fig. 9), where the DQPT is absent. It is clear that the PGP $\phi_k^G(t)$ is analytic on the (k, t) plane, and its winding number $v_D(t)$ is a continuous function of time when the DQPT does not occur. All the

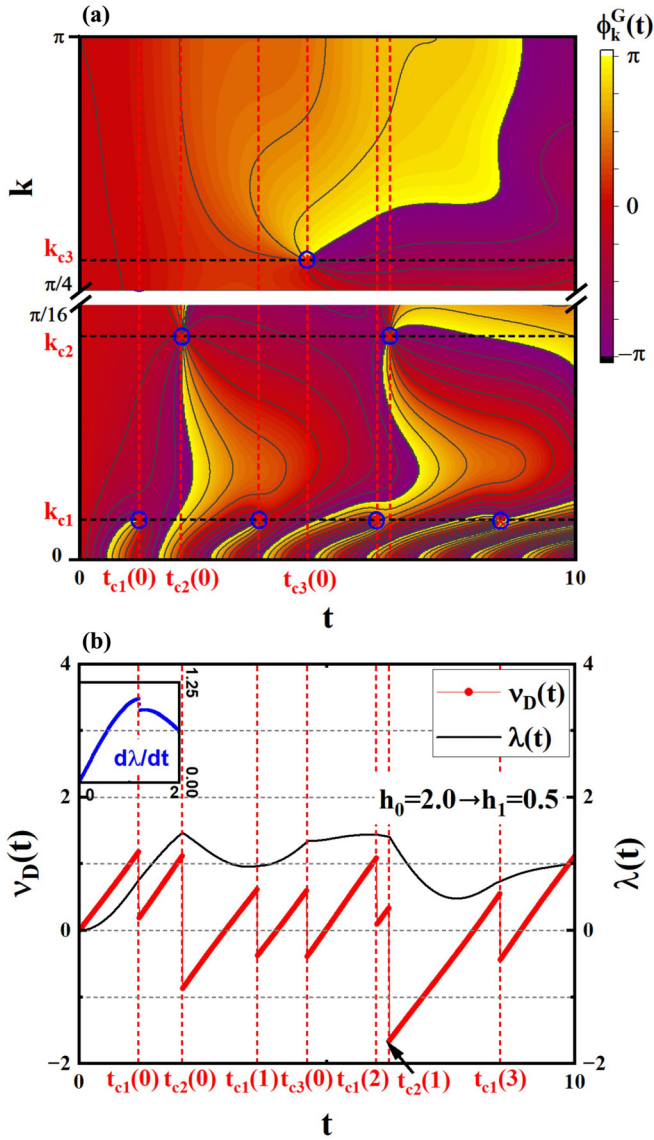


FIG. 3. (a) Contour plot of PGP $\phi_k^G(t)$ as a function of (k, t) for the quench from the PM phase to the FM phase ($h_0 = 2.0$ to $h_1 = 0.5$). The phase vortices are marked by blue circles at the critical momentum and critical times ($k_c, t_c(n)$). The red crosses denote the critical momenta and critical times obtained according to the Fisher zeros (9) and Eq. (10). (b) The winding number $v_D(t)$ and rate function $\lambda(t)$ as functions of time t . Note that the critical time $t_{c1}(0)$ is not distinguished clearly, so we use the first-order derivative $d\lambda/dt$ of the rate function to highlight the singularity (see the inset).

examples reveal that the PGP and the winding number are not topological in the periodic-2 QIC, which is different from that in homogeneous systems [11,28,48,49,51,52]. In both periodic and homogeneous systems, the discontinuous points of the winding number $v_D(t)$ and the dynamical vortices in the PGP are closely related to the critical times of the DQPTs, and they occur when the Loschmidt amplitude equals zero.

In previous works in which the homogeneous systems were intensively studied [11,28,48,49,51,52], the winding number $v_D(t)$ itself was integer quantized, and so were the

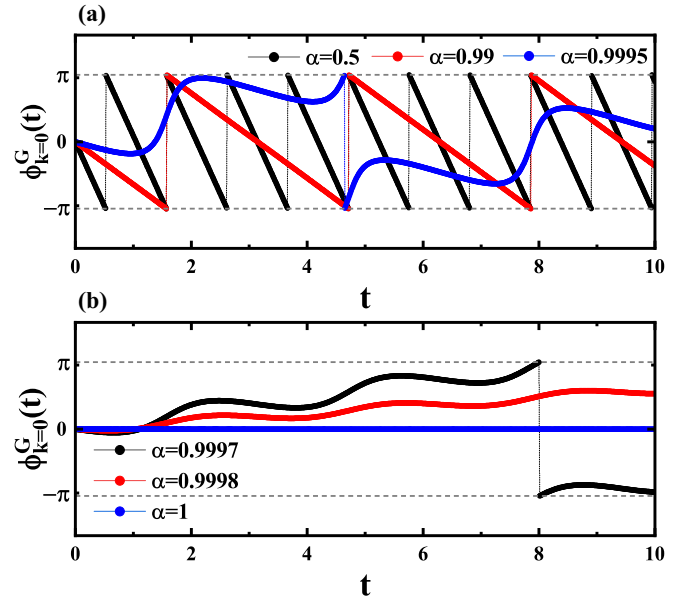


FIG. 4. Factor components $\phi_{k=0}^G(t)$ for different parameters α in the case of quench from the PM phase to the FM phase ($h_0 = 2.0$ to $h_1 = 0.5$). (a) The speed of oscillation tends to decrease with α from 0.5 to 1. (b) In particular, the oscillation period goes to the infinity as α approaches unity, and $\phi_{k=0}^G(t)$ is zero for the homogeneous system ($\alpha = 1$).

discontinuous jumps of $v_D(t)$ at the critical time of the DQPT. The quantized jumps of $v_D(t)$ at DQPTs are also observed in period-2 QIC, but $v_D(t)$ is no longer quantized. The discrepancy between these two types of quantization can be traced back to different physical origins. The quantization of the jump is protected by the dynamical vortex of the PGP in (k, t) space. The PGP diverges at the dynamical vortex where the Loschmidt amplitude $\mathcal{G}(t) = r(t)e^{i(\phi^G(t) + \phi^{\text{dyn}}(t))}$ vanishes and its phase is ill defined. However, according to Eq. (15), both the boundary term and the jump term contribute to the winding number. Although the jump term always provides quantized contributions as just explained, the boundary term $[\phi_{k=\pi}^G(t) - \phi_{k=0}^G(t)]$ is not necessarily quantized in general. For example, in the period-2 QIC, the PGP exhibits different behaviors as time is changed at the boundary of the half Brillouin zone ($k = 0$ and $k = \pi$) in the presence of periodic modulation.

To illustrate the effect of periodic modulation, we show the factor component $\phi_{k=0}^G(t)$ for different parameters α in Fig. 4, where $\alpha = 1$ corresponds to the homogeneous system. It is clear that $\phi_{k=0}^G(t)$ oscillates with time in the periodic QIC, and the speed of oscillation tends to decrease with α from 0.5 to 1 [see Figs. 4(a) and 4(b)]. In particular, $\phi_{k=0}^G(t)$ is zero in the homogeneous system ($\alpha = 1$). Therefore, we conclude that the PGP changing with time at the boundaries of the half Brillouin zone results from the periodic modulation. Actually, the change in the PGP with time at the boundary of the half Brillouin zone is also observed in the periodic Kitaev chain [47]. Therefore, it is inferred that the winding number in the periodic Kitaev chain is not quantized either.

III. DISORDERED QUANTUM SPIN CHAINS

In this section, we extend the PGP to disordered systems. The Hamiltonian of the QIC with disordered hopping interactions is

$$H = -\frac{1}{2} \sum_{n=1}^N J_n \sigma_n^x \sigma_{n+1}^x - \frac{h}{2} \sum_{n=1}^N \sigma_n^z, \quad (16)$$

where $J_n = J + \Delta J_n$ are the hopping interactions between the nearest-neighbor spins. ΔJ_n are independent random numbers distributed uniformly in the interval $[-w/2, w/2]$ with the strength of disorder w . For convenience, we take $J = 1$ without loss of generality.

By using the Jordan-Wigner and Bogoliubov transformations [71,72], the Hamiltonian in Eq. (16) can be reduced to the diagonal form (see Appendix B 1)

$$H = \sum_n \Lambda_n \left(\eta_n^\dagger \eta_n - \frac{1}{2} \right) \quad (17)$$

in real space, where η_n^\dagger and η_n are fermionic creation and annihilation operators and Λ_n is the excitation energy for n quasiparticle mode.

The ground state is $|\text{GS}\rangle = \bigotimes_n |0_n\rangle$ in real space, where $|0_n\rangle (n = 1, \dots, N)$ denotes the vacuum state in the quasiparticle mode Λ_n , i.e., $\eta_n |0_n\rangle = 0$. The ground-state energy is given by

$$E_0 = -\sum_{n=1}^N \frac{1}{2} \Lambda_n. \quad (18)$$

We study the quantum quench from $H_0 = H(h_0)$ to $\tilde{H} = H(h_1)$, where the initial state $|\psi_0\rangle = |\text{GS}\rangle$ is taken as the ground state of the prequench Hamiltonian. Therefore, the time-evolved state at arbitrary time after quench is given by

$$|\psi(t)\rangle = e^{-i\tilde{H}t} |\psi_0\rangle. \quad (19)$$

Considering the relation between the ground states of the pre- and postquench [33,73], we have

$$|\psi_0\rangle = \frac{1}{\mathcal{N}} \exp\left(\frac{1}{2} \sum_{mn} \tilde{\eta}_m^\dagger G_{mn} \eta_n^\dagger\right) |\tilde{\psi}_0\rangle, \quad (20)$$

where $|\tilde{\psi}_0\rangle = |\tilde{\text{GS}}\rangle$ is the ground state of the postquench Hamiltonian. Therefore, we obtain the Loschmidt amplitude and decompose $\mathcal{G}(t) = \langle \psi_0 | \psi(t) \rangle = e^{-i\tilde{E}_0 t} \prod_{m=1}^{N-1} \mathcal{G}_m(t)$ for every quasiparticle mode Λ_m , with

$$\mathcal{G}_m(t) = e^{-i\tilde{E}_{0m} t} \prod_{n>m} \frac{1}{\mathcal{N}_{mn}^2} [1 + e^{-i(\tilde{\Lambda}_m + \tilde{\Lambda}_n)t} |G_{mn}|^2] \quad (21)$$

in real space, where $\mathcal{N}_{mn}^2 = 1 + |G_{mn}|^2$ is the normalization coefficient (see Appendix B 2). The associated Fisher zeros of the Loschmidt amplitude can be calculated by $\mathcal{G}(z) = 0$, that is,

$$z_j = \frac{1}{\tilde{\Lambda}_m + \tilde{\Lambda}_n} [\ln |G_{mn}|^2 + i(2j+1)\pi], \quad j \in \mathbb{N}. \quad (22)$$

According to Eq. (22), we obtain the condition for the occurrence of the DQPT and the critical times as

$$|G_{mn}| = 1, \quad t_c(j) = \frac{(2j+1)\pi}{\tilde{\Lambda}_m + \tilde{\Lambda}_n}. \quad (23)$$

Similar to Eq. (11), in polar coordinates, the factor of the Loschmidt amplitude is given by

$$\begin{aligned} \mathcal{G}_m(t) &= \text{Re}[\mathcal{G}_m(t)] + i\text{Im}[\mathcal{G}_m(t)] \\ &= r_m(t) e^{i\phi_m(t)} = r_m(t) e^{i[\phi_m^{\text{dyn}}(t) + \phi_m^G(t)]}, \end{aligned} \quad (24)$$

with the modulus $r_m(t) = \sqrt{\text{Re}[\mathcal{G}_m(t)]^2 + \text{Im}[\mathcal{G}_m(t)]^2}$ and the argument $\phi_m(t) = \arg[\mathcal{G}_m(t)]$. The associated dynamical phase $\phi_m^{\text{dyn}}(t)$ is

$$\phi_m^{\text{dyn}}(t) = -\int_0^t ds \langle \psi(s) | \tilde{H}_m | \psi(s) \rangle = \left(\frac{1}{2} - p_m\right) \tilde{\Lambda}_m t, \quad (25)$$

with

$$p_m = \frac{\sum_{n>m} |G_{mn}|^2}{\prod_{n>m} (1 + |G_{mn}|^2)}. \quad (26)$$

Therefore, the PGP in the disordered QIC can be calculated by

$$\phi_m^G(t) = \phi_m(t) - \phi_m^{\text{dyn}}(t). \quad (27)$$

In the following, we will show two typical examples to illustrate the PGP $\phi_m^G(t)$ in the disordered QIC with weak disorder, so that there is only one extra group of DQPTs induced by the weak disorder in the system [33].

A. Numerical results

To illustrate the effect of the weak disorder on the DQPT, we show the rate functions for the weakly disordered QIC ($w = 0.001$) and the homogeneous QIC ($w = 0$) in Fig. 5. The quench path in Fig. 5(a) is from $h_0 = 0.5$ to $h_1 = 1.5$. It can be seen that the homogeneous QIC has critical times $t_{c1}(n) = (2n+1)t_{c1}(0)$, $t_{c1}(0) \approx 1.99$ [see the blue line in Fig. 5(a)]. However, the system has one more group of critical times in the presence of weak disorder, where the new critical times induced by the disorder are given by $t_{c2}(n) = (2n+1)t_{c2}(0)$, $t_{c2}(0) \approx 3.14$. Similar behaviors are also observed in Fig. 5(b), where the quench path is from $h_0 = 1.5$ to $h_1 = 0.5$. The homogeneous QIC has only one group of critical times, $t_{c1}(n) = (2n+1)t_{c1}(0)$, $t_{c1}(0) \approx 2.57$, and the new extra critical times emerge in the disordered QICs, which are given by $t_{c2}(n) = (2n+1)t_{c2}(0)$, $t_{c2}(0) \approx 3.13$. Note that we display the results of three disordered samples for each quench case. It is found that the different samples influence only the values of the rate functions and do not change the critical times of the DQPT. The critical times are generally determined by the disorder strength w , which has been tested for several values. Therefore, in our work, we do not need to average over large numbers of disordered configurations, which greatly reduces our workload.

Unlike the case in the periodic QIC, the PGP cannot be decomposed into every momentum k due to the lack of lattice translation invariance. However, we can decompose the PGP into the quasiparticle mode Λ_m in real space according to Eqs. (24), (25), and (27). In Fig. 6, we show the contour plot of

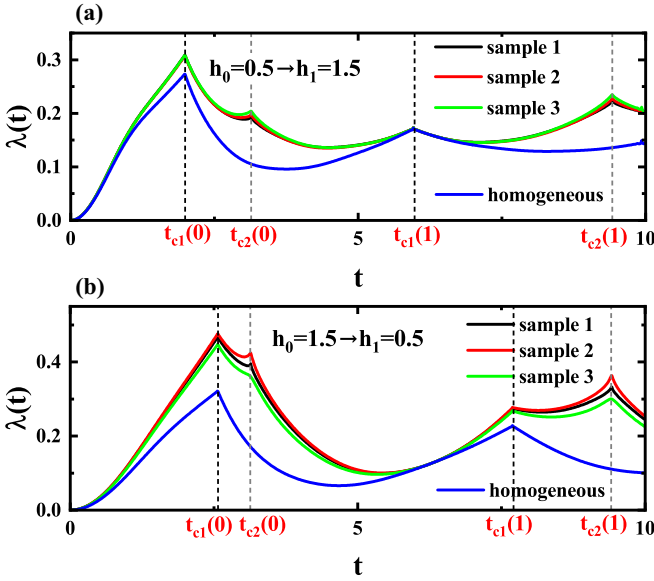


FIG. 5. Rate functions in the disordered QIC with strength of disorder $w = 0.001$. The quench path in (a) is from $h_0 = 0.5$ to $h_1 = 1.5$, and that in (b) is from $h_0 = 1.5$ to $h_1 = 0.5$. For each case, we give results for three disorder samples. It can be seen that different weakly disordered samples influence only the values of rate functions and do not change the critical times. For comparison, we also display the rate function of the homogeneous QIC ($w = 0$). It is clear that new critical times $t_{c2}(n)$, $n = 0, 1, \dots$ of DQPTs emerge in the presence of weak disorder. The system size is $N = 1000$.

the PGP $\phi_m^G(t)$ for the quench from $h_0 = 0.5$ to $h_1 = 1.5$ in the (m, t) plane, in analogy with the (k, t) plane in the period-2 QIC. We mark the two dynamical vortices by blue circles, which are consistent with the critical times $t_{c1}(0)$ and $t_{c2}(0)$ calculated according to Eq. (23) [see Fig. 6(b)]. Typically, the dynamical vortices are related to the nonanalytic contribution to the PGP from one specific component, $\phi_m^G(t)$. To find those singular components, we analyze the quasiparticle modes near the dynamical vortices and find that the nonanalytic point of $\phi_{m=1}^G(t)$ corresponds to the critical time $t_{c2}(0)$ and that of $\phi_{m=161}^G(t)$ corresponds to the critical time $t_{c1}(0)$ [see Fig. 6(a)].

Similarly, we study the PGP $\phi_m^G(t)$ for the quench from $h_0 = 1.5$ to $h_1 = 0.5$ (see Fig. 7). Two dynamical vortices exist at the critical times $t_{c1}(0)$ and $t_{c2}(0)$ [see Fig. 7(b)]. According to Fig. 7(a), the critical times $t_{c1}(0)$ and $t_{c2}(0)$ are induced by the nonanalytic points of $\phi_{m=161}^G(t)$ and $\phi_{m=3}^G(t)$, respectively.

To summarize this section, we reformulate the PGP in real space, which allows us to study the PGP in the disordered QIC where the momentum is not a good quantum number. We observe the DQPT independently not only from the rate function but also from the dynamical vortices of PGP in the (m, t) plane. The consistency of the two methods confirms the validity of our approach. It is found that the disorder induces new DQPTs in addition to those from the homogeneous QIC, and the new DQPTs are also accompanied by the nonanalytic singularities of the PGP. Recall that in the periodic QIC, the nonanalytic singularities of the PGP occur when the modulus

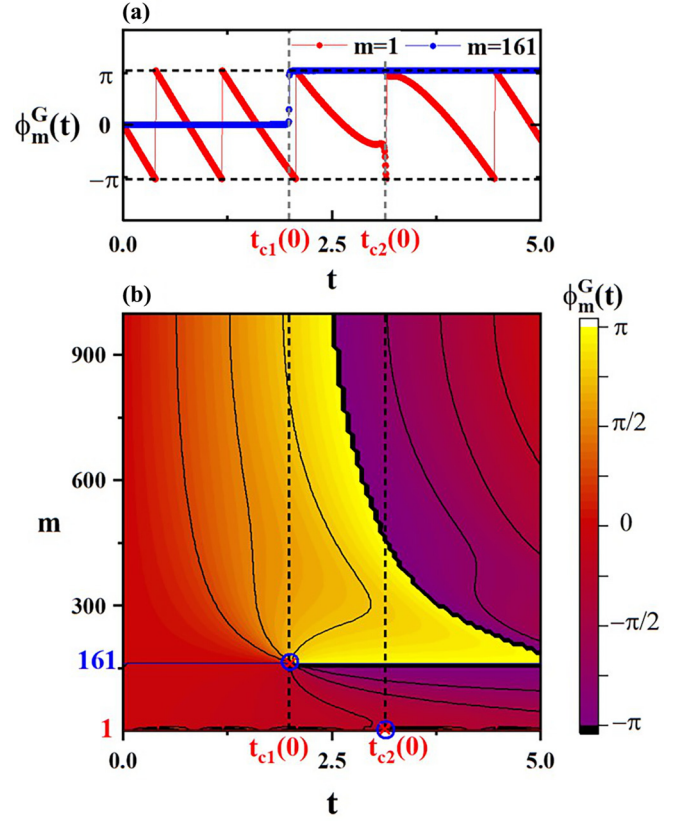


FIG. 6. (a) The factor components of the PGP $\phi_m^G(t)$ for $m = 1$ (red lines) and $m = 161$ (blue lines) in the disordered QIC with $w = 0.001$. The quench path is from $h_0 = 0.5$ to $h_1 = 1.5$. It can be seen that $\phi_{m=1}^G(t)$ and $\phi_{m=161}^G(t)$ show nonanalytic singularity at the critical times $t_{c2}(0) \approx 3.14$ and $t_{c1}(0) \approx 1.99$, respectively. (b) The contour plot of the PGP $\phi_m^G(t)$ in the (m, t) plane. There are two dynamical vortices, circled in blue, corresponding to critical times $t_{c1}(0) \approx 1.99$ and $t_{c2}(0) \approx 3.14$. The red crosses denote the critical momenta and critical times obtained according to Eq. (23).

of the Loschmidt amplitude equals zero. Likewise, this is also the case in the disordered QIC.

IV. CONCLUSION

In this paper, we investigated the PGP in periodic and disordered QICs after a sudden quench. In the period-2 QIC, we found that the winding numbers $\nu_D(t)$ are not quantized and thus not topological. By comparing the results of the periodic QIC with that in the homogeneous system, we clarified that the non-integer-quantized winding numbers result from the periodic modulation, which can dramatically change the behavior of the PGP at the boundary of the half Brillouin zone. Nevertheless, the PGP still manifests nonanalytic singularities at the critical times of the DQPT. This clarifies that the standard definition of the winding number can no longer serve as a topological quantum number in the period-2 QIC. Furthermore, we gave a general expression to calculate the PGP in real space, which allowed us to investigate the PGP in the disordered QIC. Although the disorder breaks the translational invariance, we can calculate the PGP by collecting the contribution from every quasiparticle mode Λ_m in real space.

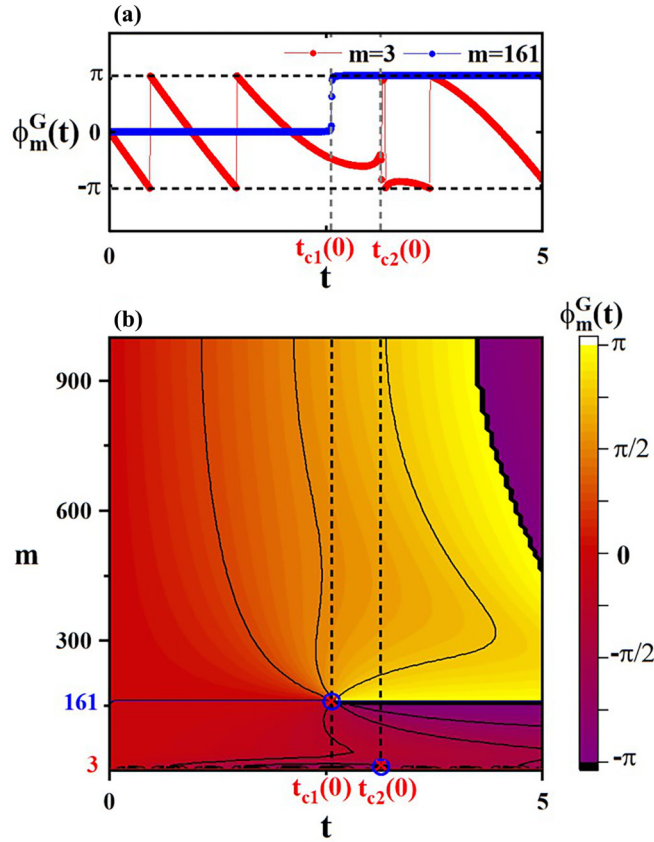


FIG. 7. (a) The factor components of the PGP $\phi_m^G(t)$ for $m = 3$ (red lines) and $m = 161$ (blue lines) in the disordered QIC with $w = 0.001$. The quench path is from $h_0 = 1.5$ to $h_1 = 0.5$. It can be seen that $\phi_{m=3}^G(t)$ and $\phi_{m=161}^G(t)$ show nonanalytic singularity at the critical times $t_{c2}(0) \approx 3.13$ and $t_{c1}(0) \approx 2.57$, respectively. (b) The contour plot of the PGP $\phi_m^G(t)$ in the (m, t) plane. There are two dynamical vortices, circled in blue, corresponding to the critical times $t_{c1}(0) \approx 2.57$ and $t_{c2}(0) \approx 3.13$. The red crosses denote the critical momenta and critical times obtained according to Eq. (23).

We found that all the critical times, including the one induced by weak disorder, of the DQPTs in the disordered QIC have a one-to-one correspondence with the nonanalytic points of the PGP. From our results, the DQPT and the nonanalytic behavior of the PGP are closely related in all three cases, the homogeneous, periodic, and disordered systems, regardless of whether the winding number is quantized (topological).

Finally, we emphasize that the one-to-one correspondence between the nonanalytic singularity of the PGP and the DQPT is because they both occur when the modulus $r(t)$ of the

Loschmidt amplitude $\mathcal{G}(t) = r(t)e^{i(\phi^G(t) + \phi^{\text{dyn}}(t))}$ vanishes. Our work reveals the essential connection between the DQPT and the nonanalytic behavior of the geometric phase, which is of great help for understanding the general properties of the quantum system in the short-term dynamical process. Meanwhile, we also recognize the limitations of using the winding number as dynamical topological order parameters to describe DQPTs, which calls for a new dynamical order parameter to characterize the notion of phase and phase transitions out of equilibrium.

ACKNOWLEDGMENTS

K.C. acknowledges Prof. P. Tong, Prof. H. Guo, and Z. Hou for extensive discussions and critical comments on the manuscript. The work is supported by the National Key Basic Research Program of China (Grant No. 2020YFB0204800), the National Science Foundation of China (Grant No. 12204432), and the Key Research Projects of Zhejiang Lab (Grants No. 2021PB0AC01 and No. 2021PB0AC02).

APPENDIX A: PERIOD-2 QIC

1. Diagonalization of the period-2 QIC

For the period-2 QIC (3), by applying the Jordan-Wigner transformation $\sigma_n^+ = c_n^\dagger e^{i\pi \sum_{m<n} c_m^\dagger c_m}$, $\sigma_n^- = e^{-i\pi \sum_{m<n} c_m^\dagger c_m} c_n$, and $\sigma_n^z = 2c_n^\dagger c_n - 1$ with spin raising and lowering operators $\sigma_n^\pm = (\sigma_n^x \pm i\sigma_n^y)/2$, we obtain a spinless Fermion model [74–77],

$$H = -\frac{1}{2} \sum_{n=1}^N \{ [J_n(c_n^\dagger c_{n+1} + c_n^\dagger c_{n+1}^\dagger) + hc_n^\dagger c_n] + \text{H.c.} \}. \quad (\text{A1})$$

Note that $\{J_n\}$ is a period-2 sequence, so the Hamiltonian (A1) can be mapped in the complex lattices ($N' = N/2$),

$$H = -\frac{1}{2} \sum_{n=1}^{N'} \{ [J(a_n^\dagger b_n + a_n^\dagger b_n^\dagger) + ha_n^\dagger a_n] + [\alpha J(b_n^\dagger a_{n+1} + b_n^\dagger a_{n+1}^\dagger) + hb_n^\dagger b_n] + \text{H.c.} \}, \quad (\text{A2})$$

where $a_{2l-1} \mapsto c_{2l-1}$ and $b_{2l} \mapsto c_{2l}$ ($l \in \mathbb{Z}$). The Hamiltonian (A2) contains the superconductor terms $a_n^\dagger b_n^\dagger$ and $b_n^\dagger a_{n+1}^\dagger$, which ensure that the parity of the number of fermions is conserved. After a Fourier transformation with $a_n = \frac{1}{\sqrt{N'}} \sum_k e^{ikn} a_k$ and $b_n = \frac{1}{\sqrt{N'}} \sum_k e^{ikn} b_k$, the superconductor terms give the terms $a_k^\dagger b_{-k}^\dagger$ and $b_k^\dagger a_{-k}^\dagger$ in momentum space. The Hamiltonian thus takes the form $H = \sum_{k>0} \Psi_k^\dagger H_k \Psi_k$ in the half Brillouin zone $k \in (0, \pi]$, with the spinor operator $\Psi_k^\dagger = (a_k^\dagger, a_{-k}, b_k^\dagger, b_{-k})$ and

$$H_k = \frac{J}{2} \begin{pmatrix} -2h/J & 0 & -(1 + \alpha e^{-ik}) & -(1 - \alpha e^{-ik}) \\ 0 & 2h/J & (1 - \alpha e^{-ik}) & (1 + \alpha e^{-ik}) \\ -(1 + \alpha e^{ik}) & (1 - \alpha e^{ik}) & -2h/J & 0 \\ -(1 - \alpha e^{ik}) & (1 + \alpha e^{ik}) & 0 & 2h/J \end{pmatrix}. \quad (\text{A3})$$

The factor H_k is obviously a Hermitian matrix, which can be diagonalized to the form $H_k = Z\Lambda Z^\dagger$ with diagonal matrix $\Lambda_k = \text{diag}(\Lambda_{k1}, -\Lambda_{k1}, \Lambda_{k2}, -\Lambda_{k2})$. By defining the canonical transformation

$$\Theta_k^\dagger = (\eta_{k1}^\dagger, -\eta_{k1}, \eta_{k2}^\dagger, -\eta_{k2}) = (a_k^\dagger, a_{-k}, b_k^\dagger, b_{-k})Z, \quad (\text{A4})$$

we obtain the Hamiltonian in diagonal form,

$$H = \sum_{k>0} \Theta_k^\dagger \Lambda_k \Theta_k. \quad (\text{A5})$$

Furthermore, the canonical transformation (A4) can be expressed as

$$\begin{pmatrix} \Gamma_k \\ \Gamma_k^{\dagger T} \end{pmatrix} = \begin{pmatrix} U(k) & V(k) \\ V^*(k) & U^*(k) \end{pmatrix} \begin{pmatrix} \Phi_k \\ \Phi_k^{\dagger T} \end{pmatrix} = M \begin{pmatrix} \Phi_k \\ \Phi_k^{\dagger T} \end{pmatrix}, \quad (\text{A6})$$

where $\Gamma_k = (\eta_{k1}, \eta_{-k1}, \eta_{k2}, \eta_{-k2})^T$ and $\Phi_k = (a_k, a_{-k}, b_k, b_{-k})^T$.

2. Loschmidt amplitude in the period-2 QIC

We study the quantum quench from $H_0 = H(h_0)$ to $\tilde{H} = H(h_1)$. According to Eq. (A6), the canonical transformation between the quasiparticle operators of pre- and postquench Hamiltonians is given by

$$\begin{aligned} \begin{pmatrix} \Gamma_k \\ \Gamma_k^{\dagger T} \end{pmatrix} &= M\tilde{M}^{-1} \begin{pmatrix} \tilde{\Gamma}_k \\ \tilde{\Gamma}_k^{\dagger T} \end{pmatrix} \\ &= \begin{pmatrix} U\tilde{U}^\dagger + V\tilde{V}^\dagger & U\tilde{V}^T + V\tilde{U}^T \\ U^*\tilde{V}^\dagger + V^*\tilde{U}^\dagger & U^*\tilde{U}^T + V^*\tilde{V}^T \end{pmatrix} \begin{pmatrix} \tilde{\Gamma}_k \\ \tilde{\Gamma}_k^{\dagger T} \end{pmatrix}. \end{aligned} \quad (\text{A7})$$

By considering the quasiparticle ground states satisfying $\eta_{k\mu}|\psi_{0k}\rangle = 0$ and $\tilde{\eta}_{k\mu}|\tilde{\psi}_{0k}\rangle = 0$, we can express the ground state $|\psi_{0k}\rangle$ of the prequench Hamiltonian as a superposition of the ground state $|\tilde{\psi}_{0k}\rangle$ for the postquench Hamiltonian,

$$\begin{aligned} |\psi_{0k}\rangle &= \frac{1}{\mathcal{N}} \exp\left[\frac{1}{2}\tilde{\Gamma}_k^\dagger G \tilde{\Gamma}_k^{\dagger T}\right] |\tilde{\psi}_{0k}\rangle \\ &= \frac{1}{\mathcal{N}} \prod_{\mu,v=1}^2 (1 + G_{k\mu,-kv} \eta_{k\mu}^\dagger \eta_{-kv}^\dagger) |\tilde{\psi}_{0k}\rangle, \end{aligned} \quad (\text{A8})$$

where $G = -(U\tilde{U}^\dagger + V\tilde{V}^\dagger)^{-1}(U\tilde{V}^T + V\tilde{U}^T)$. According to Pauli's exclusion principle of fermions and momentum

conservation, the matrix G has nonzero elements $G_{k\mu,-kv}$, that is,

$$G = \begin{pmatrix} 0 & G_{k1,-k1} & 0 & G_{k1,-k2} \\ -G_{k1,-k1} & 0 & G_{k2,-k1} & 0 \\ 0 & -G_{k2,-k1} & 0 & G_{k2,-k2} \\ -G_{k1,-k2} & 0 & -G_{k2,-k2} & 0 \end{pmatrix}. \quad (\text{A9})$$

Therefore, we can obtain the Loschmidt amplitude $\mathcal{G}(t) = \prod_{k>0} \mathcal{G}_k(t)$, with

$$\mathcal{G}_k(t) = \frac{e^{-i\tilde{E}_{0k}t}}{\mathcal{N}^2} \prod_{\mu,v=1}^2 [1 + |G_{k\mu,-kv}|^2 e^{i(\tilde{\Lambda}_{k\mu} + \tilde{\Lambda}_{-kv})t}], \quad (\text{A10})$$

where $\mathcal{N} = \prod_{\mu,v=1}^2 \mathcal{N}_{k\mu,-kv} = \prod_{\mu,v=1}^2 \sqrt{1 + |G_{k\mu,-kv}|^2}$ is the normalization coefficient.

3. PGP in period-2 QIC

In polar coordinates, we have

$$\begin{aligned} \mathcal{G}_k(t) &= \text{Re}[\mathcal{G}_k(t)] + i\text{Im}[\mathcal{G}_k(t)] \\ &= r_k(t)e^{i\phi_k(t)} = r_k(t)e^{i[\phi_k^{\text{dyn}}(t) + \phi_k^{\mathcal{C}}(t)]}, \end{aligned} \quad (\text{A11})$$

where $\text{Re}[\mathcal{G}_k(t)]$ and $\text{Im}[\mathcal{G}_k(t)]$ are the real and imaginary parts of $\mathcal{G}_k(t)$. Therefore, the modulus $r_k(t)$ of $\mathcal{G}_k(t)$ is given by

$$r_k(t) = \sqrt{\text{Re}[\mathcal{G}_k(t)]^2 + \text{Im}[\mathcal{G}_k(t)]^2}. \quad (\text{A12})$$

The argument $\phi_k(t)$ of $\mathcal{G}_k(t)$ is

$$\phi_k(t) = \arg[\mathcal{G}_k(t)] \in (-\pi, \pi], \quad (\text{A13})$$

where we follow the standard form

$$\arg[\mathcal{G}_k(t)] = \begin{cases} \arctan \frac{y}{x}, & x > 0, \\ \frac{\pi}{2}, & x = 0, y > 0, \\ -\frac{\pi}{2}, & x = 0, y < 0, \\ \pi + \arctan \frac{y}{x}, & x < 0, y > 0, \\ \arctan \frac{y}{x} - \pi, & x < 0, y < 0, \\ 0, & x > 0, y = 0, \\ \pi, & x < 0, y = 0, \\ \text{not defined,} & x = 0. \end{cases} \quad (\text{A14})$$

with $x = \text{Re}[\mathcal{G}_k(t)]$ and $y = \text{Im}[\mathcal{G}_k(t)]$.

The dynamical phase $\phi_k^{\text{dyn}}(t)$ is defined as [11]

$$\begin{aligned} \phi_k^{\text{dyn}} &= -\int_0^t ds \langle \psi_k(s) | \tilde{H}_k | \psi_k(s) \rangle = -\int_0^t ds \langle \psi_{0k} | e^{i\tilde{H}_k s} \tilde{H}_k e^{-i\tilde{H}_k s} | \psi_{0k} \rangle = -\int_0^t ds \langle \psi_{0k} | \tilde{H}_k | \psi_{0k} \rangle \\ &= -t \langle \psi_{0k} | \left[\tilde{\Lambda}_{k1} \left(\tilde{\eta}_{k1}^\dagger \tilde{\eta}_{k1} - \frac{1}{2} \right) + \tilde{\Lambda}_{-k1} \left(\tilde{\eta}_{-k1}^\dagger \tilde{\eta}_{-k1} - \frac{1}{2} \right) + \tilde{\Lambda}_{k2} \left(\tilde{\eta}_{k2}^\dagger \tilde{\eta}_{k2} - \frac{1}{2} \right) + \tilde{\Lambda}_{-k2} \left(\tilde{\eta}_{-k2}^\dagger \tilde{\eta}_{-k2} - \frac{1}{2} \right) \right] | \psi_{0k} \rangle \\ &= -t [\tilde{\Lambda}_{k1} \langle \psi_{0k} | \tilde{\eta}_{k1}^\dagger \tilde{\eta}_{k1} + \tilde{\eta}_{-k1}^\dagger \tilde{\eta}_{-k1} | \psi_{0k} \rangle + \tilde{\Lambda}_{k2} \langle \psi_{0k} | \tilde{\eta}_{k2}^\dagger \tilde{\eta}_{k2} + \tilde{\eta}_{-k2}^\dagger \tilde{\eta}_{-k2} | \psi_{0k} \rangle] - \tilde{E}_{0k}t, \end{aligned} \quad (\text{A15})$$

where $\tilde{E}_{0k} = -(\tilde{\Lambda}_{k1} + \tilde{\Lambda}_{k2})$. From Eq. (A8), we have

$$\begin{aligned} p_{k1,k1} &= \langle \psi_{0k} | \tilde{\eta}_{k1}^\dagger \tilde{\eta}_{k1} | \psi_{0k} \rangle \\ &= \langle \tilde{\psi}_{0k} | \frac{1}{\mathcal{N}_{k1,-k1}^2} \frac{1}{\mathcal{N}_{k1,-k2}^2} (1 + G_{k1,-k2}^* \tilde{\eta}_{-k2} \tilde{\eta}_{k1}) (1 + G_{k1,-k1}^* \tilde{\eta}_{-k1} \tilde{\eta}_{k1}) \tilde{\eta}_{k1}^\dagger \tilde{\eta}_{k1} (1 + G_{k1,-k1} \tilde{\eta}_{k1}^\dagger \tilde{\eta}_{-k1}^\dagger) (1 + G_{k1,-k2} \tilde{\eta}_{k1}^\dagger \tilde{\eta}_{-k2}^\dagger) | \tilde{\psi}_{0k} \rangle \\ &= \frac{|G_{k1,-k1}|^2 + |G_{k1,-k2}|^2}{(1 + |G_{k1,-k1}|^2)(1 + |G_{k1,-k2}|^2)}. \end{aligned} \quad (\text{A16})$$

Similarly, we obtain

$$p_{k1,k1} = \frac{|G_{k1,-k1}|^2 + |G_{k1,-k2}|^2}{(1 + |G_{k1,-k1}|^2)(1 + |G_{k1,-k2}|^2)}, \quad (\text{A17})$$

$$p_{-k1,-k1} = \frac{|G_{k1,-k1}|^2 + |G_{-k1,k2}|^2}{(1 + |G_{k1,-k1}|^2)(1 + |G_{-k1,k2}|^2)}, \quad (\text{A18})$$

$$p_{k2,k2} = \frac{|G_{-k1,k2}|^2 + |G_{k2,-k2}|^2}{(1 + |G_{-k1,k2}|^2)(1 + |G_{k2,-k2}|^2)}, \quad (\text{A19})$$

$$p_{-k2,-k2} = \frac{|G_{k1,-k2}|^2 + |G_{k2,-k2}|^2}{(1 + |G_{k1,-k2}|^2)(1 + |G_{k2,-k2}|^2)}. \quad (\text{A20})$$

By substituting Eqs. (A17), (A18), (A19), and (A20) into Eq. (A15), we have a final formula for the dynamical phase $\phi_k^{\text{dyn}}(t)$:

$$\begin{aligned} \phi_k^{\text{dyn}}(t) &= \left\{ \left[1 - \frac{2(|G_{k1,-k1}|^2 + |G_{k1,-k2}|^2)}{(1 + |G_{k1,-k1}|^2)(1 + |G_{k1,-k2}|^2)} \right] \tilde{\Lambda}_{k1} \right. \\ &\quad \left. + \left[1 - \frac{2(|G_{-k1,k2}|^2 + |G_{k2,-k2}|^2)}{(1 + |G_{-k1,k2}|^2)(1 + |G_{k2,-k2}|^2)} \right] \tilde{\Lambda}_{k2} \right\} t. \end{aligned} \quad (\text{A21})$$

Therefore, according to Eqs. (A13) and (A21), the PGP can be calculated as

$$\phi_k^G(t) = \phi_k(t) - \phi_k^{\text{dyn}}(t). \quad (\text{A22})$$

As mentioned in Sec. II A, the PGP exhibits different behaviors at the boundaries of the half Brillouin zone [see Fig. 2(a)]. Here, we show more examples of the PGPs at the boundaries of the half Brillouin zone in Fig. 8. In all the quench protocols that we have tested from the FM phase to the PM phase, we found that while $\phi_{k=0}^G(t) \approx 0$ is vanishingly small, $\phi_{k=\pi}^G(t)$ changes more rapidly with time. As a result, the time-dependent boundary contribution $\phi_{k=\pi}^G(t) - \phi_{k=0}^G(t)$ breaks the integral quantization of the winding number.

For comparison, we show $\phi_k^G(t)$ and $\nu_D(t)$ for the quench in the FM phase in Fig. 9. The quench path is from $h_0 = 0.2$ to $h_1 = 0.5$. It can be seen that $\phi_k^G(t)$ changes value in the interval $[0, 0.9]$ and does not have the nonanalytic oscillation with time (see Fig. 9). Meanwhile, from Fig. 9(b), the winding number $\nu_D(t)$ and rate function $\lambda(t)$ are smooth continuous functions with time. This clarifies that if the quench does not cross the quantum phase transition (QPT), the dynamical topological phase transition and DQPT will not occur in the period-2 QIC.

APPENDIX B: DISORDERED QIC

1. Diagonalization of the disordered QIC

Spin-1/2 quantum spin chains with nearest-neighbor interactions can generally be mapped to the spinless fermion in quadratic form via the Jordan-Wigner transformation

$$H = \sum_{mn} \left[c_m^\dagger A_{mn} c_n + \frac{1}{2} (c_m^\dagger B_{mn} c_n^\dagger + \text{H.c.}) \right], \quad (\text{B1})$$

where c_n and c_n^\dagger are the annihilation and creation operators of the fermion [78]. For system size N , matrices A and B are both $N \times N$. The Hermiticity of H demands that A is a Hermitian matrix, and anticommutation of the fermion operators

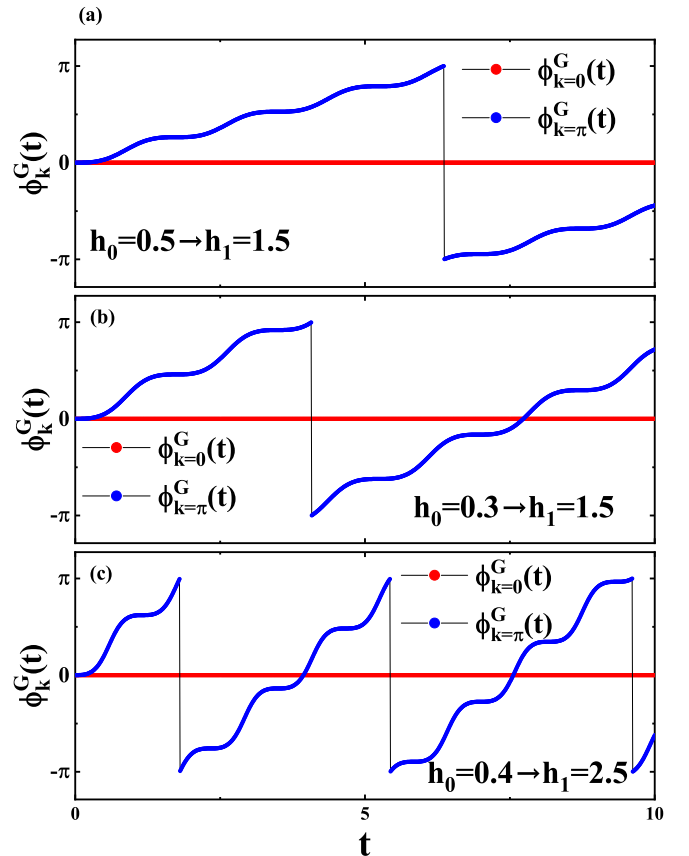


FIG. 8. Factor components of the PGP at the boundaries of the half Brillouin zone ($k = 0$ and $k = \pi$) are plotted as a function of t for several choices of quench paths from the FM phase to the PM phase. At the boundary of the half Brillouin zone, $\phi_{k=0}^G(t) \approx 0$ is almost constant. In comparison, $\phi_{k=\pi}^G(t)$ changes more significantly with time.

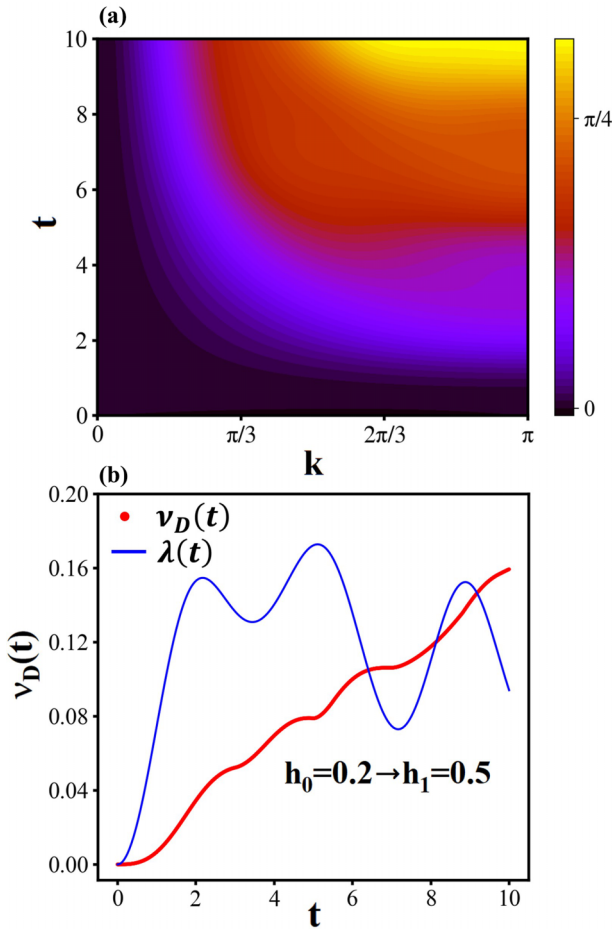


FIG. 9. (a) Color plot of $\phi_k^G(t)$ for the quench in the FM phase, without crossing the QPT. (b) Corresponding winding number $v_D(t)$ and rate function $\lambda(t)$.

demands that B is an antisymmetric matrix. Matrices A and B are given by

$$A_{mn} = -h\delta_{mn} - J_n\delta_{m,n+1}/2 - J_m\delta_{m+1,n}/2, \quad (\text{B2})$$

$$B_{mn} = -J_m\delta_{m+1,n}/2 + J_n\delta_{m,n+1}/2. \quad (\text{B3})$$

To write the Hamiltonian (B1) in the diagonal form $H = \sum_n \Lambda_n(\eta_n^\dagger \eta_n - \frac{1}{2})$, we can use the Bogoliubov transformation in real space,

$$\eta_m = \sum_n (U_{mn}c_n + V_{mn}c_n^\dagger), \quad (\text{B4})$$

$$\eta_m^\dagger = \sum_{mn} (U_{mn}^*c_n^\dagger + V_{mn}^*c_n); \quad (\text{B5})$$

in matrix form it is

$$\begin{pmatrix} \eta \\ \eta^\dagger \end{pmatrix} = M \begin{pmatrix} c \\ c^\dagger \end{pmatrix} = \begin{pmatrix} U & V \\ V^* & U^* \end{pmatrix} \begin{pmatrix} c \\ c^\dagger \end{pmatrix}, \quad (\text{B6})$$

with $\eta = (\eta_1, \dots, \eta_N)^T$ and $c = (c_1, \dots, c_N)^T$. The eigenenergies of H can be obtained by solving the following eigenvalue equations:

$$\Phi(A - B)(A + B) = \Lambda^2\Phi, \quad (\text{B7})$$

$$\Psi(A + B)(A - B) = \Lambda^2\Psi, \quad (\text{B8})$$

where $\Lambda = \text{diag}(\Lambda_1, \dots, \Lambda_N)$. The matrices U and V are given by

$$U = \frac{1}{2}(\Phi + \Psi), \quad (\text{B9})$$

$$V = \frac{1}{2}(\Phi - \Psi). \quad (\text{B10})$$

2. Loschmidt amplitude in disordered QIC

We study the quantum quench from $H_0 = H(h_0)$ to $\tilde{H} = H(h_1)$. According to Eq. (B6), we have

$$\begin{aligned} \begin{pmatrix} \eta \\ \eta^\dagger \end{pmatrix} &= M\tilde{M}^{-1} \begin{pmatrix} \tilde{\eta} \\ \tilde{\eta}^\dagger \end{pmatrix} \\ &= \begin{pmatrix} U\tilde{U}^\dagger + V\tilde{V}^\dagger & U\tilde{V}^T + V\tilde{U}^T \\ U^*\tilde{V}^\dagger + V^*\tilde{U}^\dagger & U^*\tilde{U}^T + V^*\tilde{V}^T \end{pmatrix} \begin{pmatrix} \tilde{\eta} \\ \tilde{\eta}^\dagger \end{pmatrix}. \end{aligned} \quad (\text{B11})$$

By considering $\eta_n|\psi_0\rangle = 0$ and $\tilde{\eta}_n|\tilde{\psi}_0\rangle = 0$, we obtain the relation between the ground states of the pre- and postquench,

$$\begin{aligned} |\psi_0\rangle &= \frac{1}{\mathcal{N}} \exp\left(\frac{1}{2} \sum_{mn} \tilde{\eta}_m^\dagger G_{mn} \eta_n^\dagger\right) |\tilde{\psi}_0\rangle \\ &= \frac{1}{\mathcal{N}} \prod_{m,n>m} (1 + G_{mn} \tilde{\eta}_m^\dagger \eta_n^\dagger) |\tilde{\psi}_0\rangle, \end{aligned} \quad (\text{B12})$$

where $\mathcal{N} = \prod_{m,n>m} \mathcal{N}_{mn} = \prod_{m,n>m} \sqrt{1 + |G_{mn}|^2}$ is the normalization coefficient and $G = -(U\tilde{U}^\dagger + V\tilde{V}^\dagger)^{-1}(U\tilde{V}^T + V\tilde{U}^T)$ is an antisymmetrical matrix determined by only the Hamiltonian parameters. Notice that the method we use to calculate the Loschmidt amplitude in the disordered QIC is similar to that in the period-2 QIC [see Eqs. (A6), (A7), and (A8)].

According to Eq. (B12), the Loschmidt amplitude is given by

$$\begin{aligned} \mathcal{G}(t) &= \langle \psi_0 | \psi(t) \rangle = e^{-i\tilde{E}_0 t} \prod_{m=1}^{N-1} \mathcal{G}_m(t) \\ &= \frac{e^{-i\tilde{E}_0 t}}{\mathcal{N}^2} \prod_{m,n>m} [1 + e^{-i(\tilde{\Lambda}_m + \tilde{\Lambda}_n)t} |G_{mn}|^2], \end{aligned} \quad (\text{B13})$$

where

$$\mathcal{G}_m(t) = e^{-i\tilde{E}_0 t} \prod_{n>m} \frac{1}{\mathcal{N}_{mn}^2} [1 + e^{-i(\tilde{\Lambda}_m + \tilde{\Lambda}_n)t} |G_{mn}|^2] \quad (\text{B14})$$

is the component of the Loschmidt amplitude in the quasiparticle mode $\tilde{\Lambda}_m$.

3. PGP in the disordered QIC chain

In polar coordinates, we have

$$\begin{aligned} \mathcal{G}_m(t) &= \text{Re}[\mathcal{G}_m(t)] + i\text{Im}[\mathcal{G}_m(t)] \\ &= r_m(t)e^{i\phi_m(t)} = r_m(t)e^{i[\phi_m^{\text{dyn}}(t) + \phi_m^G(t)]}, \end{aligned} \quad (\text{B15})$$

where $\text{Re}[\mathcal{G}_m(t)]$ and $\text{Im}[\mathcal{G}_m(t)]$ are the real and imaginary parts of $\mathcal{G}_m(t)$. Like in the case in the period-2 QIC, the modulus $r_m(t)$ and argument $\phi_m(t)$ can also be obtained as

$$r_m(t) = \sqrt{\text{Re}[\mathcal{G}_m(t)]^2 + \text{Im}[\mathcal{G}_m(t)]^2} \quad (\text{B16})$$

and

$$\phi_m(t) = \arg[\mathcal{G}_m(t)], \quad (\text{B17})$$

respectively.

From the definition, we have

$$\begin{aligned} \phi_m^{\text{dyn}}(t) &= -\int_0^t ds \langle \psi(s) | \tilde{H}_m | \psi(s) \rangle \\ &= -t \langle \psi_0 | \tilde{H}_m | \psi_0 \rangle \\ &= -t \langle \tilde{\psi}_0 | \frac{1}{\mathcal{N}} \prod_{m', n' > m'} (1 + G_{m'n'}^* \tilde{\eta}_{n'} \tilde{\eta}_{m'}) \tilde{\Lambda}_m \left(\tilde{\eta}_m^\dagger \tilde{\eta}_m - \frac{1}{2} \right) \\ &\quad \times \frac{1}{\mathcal{N}} \prod_{m', n' > m'} (1 + G_{m'n'} \tilde{\eta}_{m'}^\dagger \tilde{\eta}_{n'}^\dagger) | \tilde{\psi}_0 \rangle \\ &= \frac{1}{2} \tilde{\Lambda}_m t - \tilde{\Lambda}_m t \langle \tilde{\psi}_0 | \frac{1}{\mathcal{N}^2} \\ &\quad \times \prod_{m', n' > m'} (1 + G_{m'n'}^* \tilde{\eta}_{n'} \tilde{\eta}_{m'}) \tilde{\eta}_m^\dagger \tilde{\eta}_m \\ &\quad \times \prod_{m', n' > m'} (1 + G_{m'n'} \tilde{\eta}_{m'}^\dagger \tilde{\eta}_{n'}^\dagger) | \tilde{\psi}_0 \rangle \\ &= \frac{1}{2} \tilde{\Lambda}_m t - \tilde{\Lambda}_m t \langle \tilde{\psi}_0 | \\ &\quad \times \prod_{n > m} \frac{1}{\mathcal{N}_{m,n}^2} (1 + G_{mn}^* \tilde{\eta}_m \tilde{\eta}_n) \tilde{\eta}_m^\dagger \tilde{\eta}_m \\ &\quad \times \prod_{n > m} (1 + G_{mn} \tilde{\eta}_m^\dagger \tilde{\eta}_n^\dagger) | \tilde{\psi}_0 \rangle \end{aligned}$$

$$\begin{aligned} &= \frac{1}{2} \tilde{\Lambda}_m t - \tilde{\Lambda}_m p_m t \\ &= \left(\frac{1}{2} - p_m \right) \tilde{\Lambda}_m t, \end{aligned} \quad (\text{B18})$$

where

$$\begin{aligned} p_1 &= \frac{\sum_{n>1} |G_{1n}|^2}{\prod_{n>1} (1 + |G_{1n}|^2)}, \\ p_2 &= \frac{\sum_{n>2} |G_{2n}|^2}{\prod_{n>2} (1 + |G_{2n}|^2)}, \\ &\quad \vdots \\ p_{N-1} &= \frac{|G_{N-1,N}|^2}{(1 + |G_{N-1,N}|^2)}. \end{aligned}$$

Therefore, the PGPs of the disordered QIC can be calculated as

$$\begin{aligned} \phi_m^G(t) &= \phi_m(t) - \phi_m^{\text{dyn}}(t) \\ &= \arg[\mathcal{G}_m(t)] - \left(\frac{1}{2} - \frac{\sum_{n>m} |G_{mn}|^2}{\prod_{n>m} (1 + |G_{mn}|^2)} \right) \tilde{\Lambda}_m t. \end{aligned} \quad (\text{B19})$$

-
- [1] D. Xiao, M.-C. Chang, and Q. Niu, *Rev. Mod. Phys.* **82**, 1959 (2010).
- [2] N. R. Cooper, J. Dalibard, and I. B. Spielman, *Rev. Mod. Phys.* **91**, 015005 (2019).
- [3] E. J. Bergholtz, J. C. Budich, and F. K. Kunst, *Rev. Mod. Phys.* **93**, 015005 (2021).
- [4] M. V. Berry, *Proc. R. Soc. London, Ser. A* **392**, 45 (1984).
- [5] B. Simon, *Phys. Rev. Lett.* **51**, 2167 (1983).
- [6] D. J. Thouless, M. Kohmoto, M. P. Nightingale, and M. den Nijs, *Phys. Rev. Lett.* **49**, 405 (1982).
- [7] A. Carollo, D. Valenti, and B. Spagnolo, *Phys. Rep.* **838**, 1 (2020).
- [8] G. Zhang and Z. Song, *Phys. Rev. Lett.* **115**, 177204 (2015).
- [9] Y. Aharonov and J. Anandan, *Phys. Rev. Lett.* **58**, 1593 (1987).
- [10] J. Samuel and R. Bhandari, *Phys. Rev. Lett.* **60**, 2339 (1988).
- [11] J. C. Budich and M. Heyl, *Phys. Rev. B* **93**, 085416 (2016).
- [12] M. Heyl, A. Polkovnikov, and S. Kehrein, *Phys. Rev. Lett.* **110**, 135704 (2013).
- [13] M. Heyl, *Rep. Prog. Phys.* **81**, 054001 (2018).
- [14] C. Karrasch and D. Schuricht, *Phys. Rev. B* **87**, 195104 (2013).
- [15] S. Vajna and B. Dóra, *Phys. Rev. B* **89**, 161105(R) (2014).
- [16] U. Divakaran, S. Sharma, and A. Dutta, *Phys. Rev. E* **93**, 052133 (2016).
- [17] K. Cao, M. Zhong, and P. Tong, *Chin. Phys. B* **31**, 060505 (2022).
- [18] M. Schmitt and S. Kehrein, *Phys. Rev. B* **92**, 075114 (2015).
- [19] F. Andraschko and J. Sirker, *Phys. Rev. B* **89**, 125120 (2014).
- [20] M. Heyl, *Phys. Rev. Lett.* **113**, 205701 (2014).
- [21] J. C. Halimeh and V. Zauner-Stauber, *Phys. Rev. B* **96**, 134427 (2017).
- [22] I. Homrighausen, N. O. Abeling, V. Zauner-Stauber, and J. C. Halimeh, *Phys. Rev. B* **96**, 104436 (2017).
- [23] T. Obuchi, S. Suzuki, and K. Takahashi, *Phys. Rev. B* **95**, 174305 (2017).
- [24] V. Zauner-Stauber and J. C. Halimeh, *Phys. Rev. E* **96**, 062118 (2017).
- [25] A. Dutta and A. Dutta, *Phys. Rev. B* **96**, 125113 (2017).
- [26] B. Žunkovič, M. Heyl, M. Knap, and A. Silva, *Phys. Rev. Lett.* **120**, 130601 (2018).
- [27] C. Karrasch and D. Schuricht, *Phys. Rev. B* **95**, 075143 (2017).
- [28] L. Zhou, Q.-H. Wang, H. Wang, and J. Gong, *Phys. Rev. A* **98**, 022129 (2018).
- [29] D. Mondal and T. Nag, *Phys. Rev. B* **106**, 054308 (2022).
- [30] M. Abdi, *Phys. Rev. B* **100**, 184310 (2019).
- [31] C. Yang, Y. Wang, P. Wang, X. Gao, and S. Chen, *Phys. Rev. B* **95**, 184201 (2017).
- [32] H. Yin, S. Chen, X. Gao, and P. Wang, *Phys. Rev. A* **97**, 033624 (2018).
- [33] K. Cao, W. Li, M. Zhong, and P. Tong, *Phys. Rev. B* **102**, 014207 (2020).
- [34] R. Modak and D. Rakshit, *Phys. Rev. B* **103**, 224310 (2021).
- [35] P. Jurcevic, H. Shen, P. Hauke, C. Maier, T. Brydges, C. Hempel, B. P. Lanyon, M. Heyl, R. Blatt, and C. F. Roos, *Phys. Rev. Lett.* **119**, 080501 (2017).

- [36] J. Zhang, G. Pagano, P. W. Hess, A. Kyprianidis, P. B. Ecker, H. Kaplan, A. V. Gorshkov, Z. X. Gong, and C. Monroe, *Nature (London)* **551**, 601 (2017).
- [37] X. Nie, B.-B. Wei, X. Chen, Z. Zhang, X. Zhao, C. Qiu, Y. Tian, Y. Ji, T. Xin, D. Lu, and J. Li, *Phys. Rev. Lett.* **124**, 250601 (2020).
- [38] K. Wang, X. Qiu, L. Xiao, X. Zhan, Z. Bian, W. Yi, and P. Xue, *Phys. Rev. Lett.* **122**, 020501 (2019).
- [39] X. Y. Xu, Q. Q. Wang, M. Heyl, J. C. Budich, W. W. Pan, Z. Chen, M. Jan, K. Sun, J. S. Xu, Y. J. Han, C. F. Li, and G. C. Guo, *Light: Sci. Appl.* **9**, 7 (2020).
- [40] T. Tian, H.-X. Yang, L.-Y. Qiu, H.-Y. Liang, Y.-B. Yang, Y. Xu, and L.-M. Duan, *Phys. Rev. Lett.* **124**, 043001 (2020).
- [41] E. A. Yuzbashyan, O. Tsypliyatyev, and B. L. Altshuler, *Phys. Rev. Lett.* **96**, 097005 (2006).
- [42] P. Barmettler, M. Punk, V. Gritsev, E. Demler, and E. Altman, *Phys. Rev. Lett.* **102**, 130603 (2009).
- [43] M. Eckstein, M. Kollar, and P. Werner, *Phys. Rev. Lett.* **103**, 056403 (2009).
- [44] B. Sciolla and G. Biroli, *Phys. Rev. Lett.* **105**, 220401 (2010).
- [45] J. Dziarmaga, *Adv. Phys.* **59**, 1063 (2010).
- [46] N. Fläschner, D. Vogel, M. Tarnowski, B. S. Rem, D. S. Lühmann, M. Heyl, J. C. Budich, L. Mathey, K. Sengstock, and C. Weitenberg, *Nat. Phys.* **14**, 265 (2018).
- [47] C. B. Mendl and J. C. Budich, *Phys. Rev. B* **100**, 224307 (2019).
- [48] S. Sharma, U. Divakaran, A. Polkovnikov, and A. Dutta, *Phys. Rev. B* **93**, 144306 (2016).
- [49] X. Qiu, T.-S. Deng, Y. Hu, P. Xue, and W. Yi, *iScience* **20**, 392 (2019).
- [50] T. V. Zache, N. Mueller, J. T. Schneider, F. Jendrzejewski, J. Berges, and P. Hauke, *Phys. Rev. Lett.* **122**, 050403 (2019).
- [51] K. Yang, L. Zhou, W. Ma, X. Kong, P. Wang, X. Qin, X. Rong, Y. Wang, F. Shi, J. Gong, and J. Du, *Phys. Rev. B* **100**, 085308 (2019).
- [52] R. Jafari and A. Akbari, *Phys. Rev. A* **103**, 012204 (2021).
- [53] L. Zhou and Q. Du, *J. Phys.: Condens. Matter* **33**, 345403 (2021).
- [54] L. Zhou and Q. Du, *New J. Phys.* **23**, 063041 (2021).
- [55] R. Jafari, A. Akbari, U. Mishra, and H. Johannesson, *Phys. Rev. B* **105**, 094311 (2022).
- [56] L.-N. Luan, M.-Y. Zhang, and L. Wang, *Phys. A (Amsterdam, Neth.)* **604**, 127866 (2022).
- [57] J. Naji, M. Jafari, R. Jafari, and A. Akbari, *Phys. Rev. A* **105**, 022220 (2022).
- [58] C. Ding, *Phys. Rev. B* **102**, 060409(R) (2020).
- [59] K. Cao, M. Zhong, and P. Tong, *J. Phys. A* **55**, 365001 (2022).
- [60] P. Tong and M. Zhong, *Phys. B (Amsterdam, Neth.)* **304**, 91 (2001).
- [61] P. Tong and M. Zhong, *Phys. Rev. B* **65**, 064421 (2002).
- [62] I. Titvinidze and G. I. Japaridze, *Eur. Phys. J. B* **32**, 383 (2003).
- [63] P. Pfeuty, *Phys. Lett. A* **72**, 245 (1979).
- [64] M. Heyl and J. C. Budich, *Phys. Rev. B* **96**, 180304(R) (2017).
- [65] S. Bhattacharjee and A. Dutta, *Phys. Rev. B* **97**, 134306 (2018).
- [66] H. Lang, Y. Chen, Q. Hong, and H. Fan, *Phys. Rev. B* **98**, 134310 (2018).
- [67] X. Qiu, T.-S. Deng, G.-C. Guo, and W. Yi, *Phys. Rev. A* **98**, 021601(R) (2018).
- [68] S. Zamani, R. Jafari, and A. Langari, *Phys. Rev. B* **102**, 144306 (2020).
- [69] M. Sadrzadeh, R. Jafari, and A. Langari, *Phys. Rev. B* **103**, 144305 (2021).
- [70] W. C. Yu, P. D. Sacramento, Y. C. Li, and H.-Q. Lin, *Phys. Rev. B* **104**, 085104 (2021).
- [71] E. Lieb, T. Schultz, and D. Mattis, *Ann. Phys. (NY)* **16**, 407 (1961).
- [72] S. Suzuki, J.-I. Inoue, and B. K. Chakrabarti, *Quantum Ising Phases and Transitions in Transverse Ising Models* (Springer, Berlin, 2013), pp. 13–46.
- [73] M. Zhong and P. Tong, *Phys. Rev. A* **84**, 052105 (2011).
- [74] R. Wakatsuki, M. Ezawa, Y. Tanaka, and N. Nagaosa, *Phys. Rev. B* **90**, 014505 (2014).
- [75] Y. Wang, J.-J. Miao, H.-K. Jin, and S. Chen, *Phys. Rev. B* **96**, 205428 (2017).
- [76] M. Ezawa, *Phys. Rev. B* **96**, 121105(R) (2017).
- [77] G. Y. Chitov, *Phys. Rev. B* **97**, 085131 (2018).
- [78] C.-B. Hua, R. Chen, D.-H. Xu, and B. Zhou, *Phys. Rev. B* **100**, 205302 (2019).

Correction: The name Zhejiang Lab was presented improperly in the affiliations and has been set right.